

Research



Cite this article: Subhedar A, Galenko PK, Varnik F. 2020 Thin interface limit of the double-sided phase-field model with convection. *Phil. Trans. R. Soc. A* **378**: 20190540. <http://dx.doi.org/10.1098/rsta.2019.0540>

Accepted: 17 February 2020

One contribution of 18 to a theme issue 'Patterns in soft and biological matters'.

Subject Areas:

computer modelling and simulation, materials science, mesoscopics, thermodynamics, computational physics

Keywords:

solidification, melt convection, phase field, asymptotic analysis

Author for correspondence:

Fathollah Varnik
e-mail: fathollah.varnik@rub.de

Thin interface limit of the double-sided phase-field model with convection


Amol Subhedar¹, Peter K. Galenko^{2,3} and Fathollah Varnik⁴

¹Institute of Materials and Processes, Karlsruhe University of Applied Sciences, Moltkestr. 30, 76133 Karlsruhe, Germany

²Physikalisch-Astronomische Fakultät, Friedrich-Schiller-Universität-Jena, 07743 Jena, Germany

³Ural Federal University, Department of Theoretical and Mathematical Physics, Laboratory of Multi-Scale Mathematical Modeling, 620000 Ekaterinburg, Russian Federation

⁴Interdisciplinary Centre for Advanced Materials Simulation, Ruhr-Universität Bochum, Universitätsstrasse 150, 44780 Bochum, Germany

 AS, 0000-0002-5322-6367; PKG, 0000-0003-2941-7742; FV, 0000-0003-2641-268X

The thin interface limit of the phase-field model is extended to include transport via melt convection. A double-sided model (equal diffusivity in liquid and solid phases) is considered for the present analysis. For the coupling between phase-field and Navier–Stokes equations, two commonly used schemes are investigated using a matched asymptotic analysis: (i) variable viscosity and (ii) drag force model. While for the variable viscosity model, the existence of a thin interface limit can be shown up to the second order in the expansion parameter, difficulties arise in satisfying no-slip boundary condition at this order for the drag force model. Nevertheless, detailed numerical simulations in two dimensions show practically no difference in dendritic growth profiles in the presence of forced melt flow obtained for the two coupling schemes. This suggests that both approaches can be used for the purpose of numerical simulations. Simulation results are also compared to analytic theory, showing excellent agreement for weak flow. Deviations at higher fluid velocities are discussed in terms of the underlying theoretical assumptions.

1. Introduction

Microstructure during solidification process forms as a complex interplay of transport processes and thermodynamical boundary conditions. Convection, in addition to the diffusion of heat and solute, adds new length and time scales to their transport. The course of solidification process can be significantly altered, and defects such as macrosegregation may be formed, by the new scales thus added. Theoretical investigations including the melt flow have been carried out previously. For different types of flow, i.e. Oseen, Stokes or potential flow, the operating state of the dendrite tip has been estimated [1–4]. Given the complexity of the free boundary problem, however, only a few cases of physical interest are tractable by theoretical means alone. Numerical solution of the coupled differential equations, in this case, offers additional insight into the problem.

In this context, phase-field models have emerged as the method of choice for the numerical study of phase transition problems [5]. In this approach, the interface is assigned a finite thickness and the thermodynamic boundary conditions on the liquid–solid interface are represented as a differential equation for a phase indicator field. Equivalence of such an approach to the sharp interface formulation, which assumes interface width W to be much smaller than all other length scales of interest, at steady state has been shown by the method of matched asymptotic analysis [6]. A major advancement in terms of the numerical efficiency of these models came with the work of Karma & Rappel [7], who performed second-order asymptotic analysis of the phase-field equations for a double-sided thermal solidification problem. They found that instead of vanishing interface thickness W , it is sufficient to have W small compared to the diffusion length of the solidification problem ($L_d = D/V$, D and V being the diffusivity of either phase and normal velocity of the interface, respectively). The thin interface limit for thermal solidification effectively accounts for the variation of the transport field across the interface. Extension of the thin interface limit to other cases of practical interest, such as solutal solidification or the one-sided model, needed an introduction of the so called anti-trapping current that removes unphysical effects such as interface stretching and jump in the diffusive field at the interface [8]. Introduction of the melt convection in the solidification process similarly poses additional challenges in terms of imposing the boundary conditions in the thin interface limit.

The frameworks which combine the melt flow with the phase-field model can roughly be classified as the variable viscosity [9,10] and the drag force model [11,12]. The variable viscosity model assumes that, within the diffuse interface, the melt fluid viscosity continues to increase and finally diverges while approaching the solid phase. Anderson *et al.* [13] analysed the variable viscosity model in the sharp interface limit. The drag force model, on the other hand, employs a dissipative force within the interfacial region with a tunable coupling parameter h [12]. This parameter plays a significant role in determining the melt velocity behaviour. It is adjusted such that the melt flow velocity matches well with the corresponding sharp interface solution for simplified geometries. The drag force coupling has been used in numerical studies of solidification phenomena with convection [14–16]. It is noteworthy that, despite the wide usage, a formal equivalence of both of these couplings in the thin interface limit (second-order asymptotics) to the sharp interface model has not been shown previously.

The present work aims at filling this gap. We provide a complete second-order asymptotic analysis of thermally driven solidification in the presence of melt convection. To keep the analysis tractable, anisotropies of the surface energy and kinetic coefficients are neglected. Diffusivities and densities of the liquid and solid phases are assumed to be identical. Furthermore, growing solid is assumed to be stationary and does not move under the forces exerted by melt flow. Special attention is paid to ensure the no-slip boundary condition. Two of the more widely used diffuse interface couplings mentioned above, namely variable viscosity model [10] and the drag force model [11] are used to analyse the fluid dynamical equations together with phase-field equations.

The two coupling schemes are compared numerically with analytical predictions in the case of two-dimensional growth of a dendrite with a forced flow in opposite direction. Only melt flow equations are analysed here and necessary temperature T and phase field φ field contributions are derived in the appendix A.

Equations for the free boundary problem of solidification are

$$\frac{\partial u}{\partial t} + \mathbf{w} \cdot \nabla u = D \nabla^2 u, \quad (1.1)$$

$$-\beta V - \delta \kappa = u, \quad V = D \left. \frac{\partial u}{\partial n} \right|_1, \quad (1.2)$$

$$\frac{\partial \mathbf{w}}{\partial t} + \mathbf{w} \cdot \nabla \mathbf{w} = -\frac{\nabla p}{\rho} + \frac{\mu_1}{\rho} \nabla^2 \mathbf{w} + (1 - \gamma u) \mathbf{g} \quad (1.3)$$

and
$$\nabla \cdot \mathbf{w} = 0, \quad \mathbf{w}_1 = 0, \quad (1.4)$$

where u is the reduced temperature field $u = (T - T_m)/L/C_p$ in the units of hypercooling L/C_p (L is latent heat and C_p is heat capacity at constant pressure), T is the temperature, T_m is the melting temperature, δ is the capillary length, β is the kinetic coefficient, \mathbf{w} is the melt velocity, ρ is the density, μ_1 is the dynamic viscosity, p is the pressure, \mathbf{g} is the acceleration due to gravity, \mathbf{w}_1 is the melt velocity at the interface (assumed to be zero). The last term on the right-hand side of equation (1.3) is due to the Boussinesq approximation and γ is a coefficient related to thermal expansion. The phase field and reduced temperature field equations are [17,18]

$$\tau \frac{\partial \varphi}{\partial t} = W^2 \nabla^2 \varphi - f'(\varphi) - A_1 \frac{W}{\delta} u g'(\varphi) \quad (1.5)$$

and

$$\frac{\partial u}{\partial t} + \mathbf{w} \cdot \nabla u = D \nabla^2 u + \frac{1}{2} \frac{\partial \varphi}{\partial t}, \quad (1.6)$$

where $f'(\varphi) = -\varphi + \varphi^3$ is the derivative of the well-known double well-potential corresponding to phase field (φ) with values $-1, 1$ in liquid and solid phases, respectively. The interpolating function $g'(\varphi)$ is $(1 - \varphi^2)^2$, τ is the phase-field relaxation time. For the melt flow, we analyse two coupling schemes. The first one is an improved drag force model [11,12]

$$\rho \left(\frac{\partial \mathbf{w}}{\partial t} + \mathbf{w} \cdot \nabla \mathbf{w} \right) = -\nabla p + \mu_1 \nabla^2 \mathbf{w} + \rho(1 - \gamma u) \mathbf{g} - h^* \mu_1 \frac{H(\varphi)}{W^2} \mathbf{w}, \quad (1.7)$$

where h^* is an optimum coupling constant and $H(\varphi)$ is interpolating polynomial with $H(\pm 1) = 0$. The second coupling scheme is a variable viscosity model [9,10]

$$\rho \left(\frac{\partial \mathbf{w}}{\partial t} + \mathbf{w} \cdot \nabla \mathbf{w} \right) = -\nabla p + \nabla \cdot (\mu(\varphi) \nabla \mathbf{w}) + \rho(1 - \gamma u) \mathbf{g}, \quad (1.8)$$

where $\mu(\varphi)$ varies across the interface as harmonic mean between liquid (μ_l) and solid viscosity ($\mu_s = \infty$) [9,10] as follows:

$$\mu(\varphi) = \frac{2\mu_l}{1 - \varphi} \quad \text{and} \quad \varphi \neq 1. \quad (1.9)$$

2. Asymptotic analysis

The small parameter for the asymptotic expansion is identified as a ratio of interface width to diffusion length, $\varepsilon = WV/D$. At the transient state of solidification process, time/length scales related to advection (due to melt flow) and diffusion can play an important role [19]. In the steady state, as in the case at hand, temperature field must be transported away from the interface at the same rate by diffusive and advective scales. In other words, the influence of melt velocity already appears in the interfacial velocity in the normal direction and thus, another small parameter related to melt convection is not necessary.

A curvilinear orthogonal system of coordinates that is attached to the moving interface, with unit vectors $\hat{\mathbf{r}}$ (normal) and $\hat{\mathbf{s}}$ (tangential) is chosen to analyse the coupled set of equations.

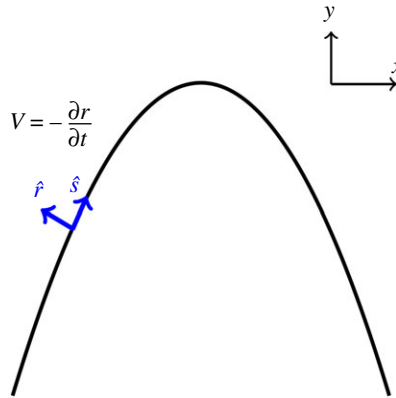


Figure 1. A curvilinear orthogonal coordinate system for a smooth interface. In this system, the unit vectors \hat{f} and \hat{s} are aligned to the directions that are perpendicular and tangential to the interface, respectively. (Online version in colour.)

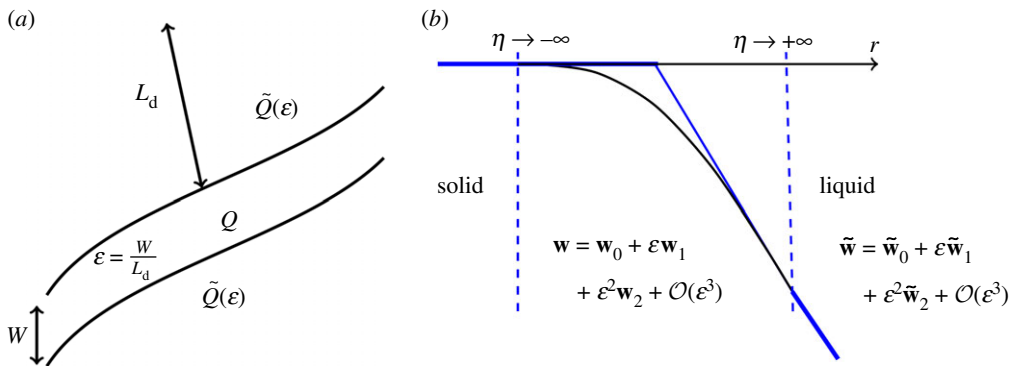


Figure 2. (a) The inner (microscopic) region corresponds to the area in the vicinity of the interface, shown here as the region of thickness W between the two parallel lines. The outer (macroscopic) region corresponds to the bulk domain. Physical variables, e.g. Q , then can be expanded in the series of ε that characterizes the smallness of the diffuse interface width. (b) The matching of the inner \mathbf{w} and outer $\tilde{\mathbf{w}}$ melt velocity field. Within each order of the successive approximation in ε , the inner and outer melt velocity should be the same while approaching the either end of the interface ($\eta \rightarrow \pm\infty$). (Online version in colour.)

Figure 1 depicts such a coordinate system. We denote the scaled length in a direction normal to the interface, r/ε , by η . The melt flow velocity and pressure are expanded for the inner (microscopic) variables up to second order in ε as (figure 2),

$$\mathbf{w} = \mathbf{w}_0 + \varepsilon \mathbf{w}_1 + \varepsilon^2 \mathbf{w}_2 \quad (2.1)$$

and

$$p = p_0 + \varepsilon p_1 + \varepsilon^2 p_2. \quad (2.2)$$

The details of asymptotics of the reduced temperature and phase field are provided in appendix A. In the present work, we will focus on the no-slip boundary condition. For this reason, only the outer (macroscopic) melt velocity $\tilde{\mathbf{w}}$ is expanded as, figure 2,

$$\tilde{\mathbf{w}} = \tilde{\mathbf{w}}_0 + \varepsilon \tilde{\mathbf{w}}_1 + \varepsilon^2 \tilde{\mathbf{w}}_2. \quad (2.3)$$

The macroscopic melt velocity can be Taylor expanded in the direction normal to the interface around the sharp interface ($r = 0$) as follows:

$$\tilde{\mathbf{w}} = \tilde{\mathbf{w}}_0(0) + \varepsilon \left(\eta \frac{\partial \tilde{\mathbf{w}}_0(0)}{\partial r} + \tilde{\mathbf{w}}_1(0) \right) + \varepsilon^2 \left(\frac{\eta^2}{2} \frac{\partial^2 \tilde{\mathbf{w}}_0(0)}{\partial r^2} + \eta \frac{\partial \tilde{\mathbf{w}}_1(0)}{\partial r} + \tilde{\mathbf{w}}_2(0) \right). \quad (2.4)$$

The principle of matched asymptotic analysis requires that the microscopic variable when matched with the macroscopic variable at either end of the interface results in the macroscopic boundary conditions. For the present case, the no-slip condition at the liquid–solid interface can be written as

$$\tilde{\mathbf{w}}_1^\pm = \tilde{\mathbf{w}}^\pm(0) = 0. \quad (2.5)$$

The superscript + (–) denotes the quantity evaluated at the interface when approached from the liquid (solid) side of the interface. $\tilde{\mathbf{w}}(0)$ reminds us that these macroscopic quantities are evaluated at the interface, $r = 0$. Matching equation (2.1) with equation (2.4) now yields

$$\tilde{\mathbf{w}}_0^\pm(0) = \lim_{\eta \rightarrow \pm\infty} \mathbf{w}_0, \quad (2.6)$$

$$\eta \frac{\partial \tilde{\mathbf{w}}_0^\pm(0)}{\partial r} + \tilde{\mathbf{w}}_1^\pm(0) = \lim_{\eta \rightarrow \pm\infty} \mathbf{w}_1 \quad (2.7)$$

and

$$\frac{\eta^2}{2} \frac{\partial^2 \tilde{\mathbf{w}}_0^\pm(0)}{\partial r^2} + \eta \frac{\partial \tilde{\mathbf{w}}_1^\pm(0)}{\partial r} + \tilde{\mathbf{w}}_2^\pm(0) = \lim_{\eta \rightarrow \pm\infty} \mathbf{w}_2. \quad (2.8)$$

We are interested in the validity of the no-slip boundary condition from the solid side of the interface. Thus we write equations (2.6)–(2.8) as

$$\tilde{\mathbf{w}}_0^-(0) = \lim_{\eta \rightarrow -\infty} \mathbf{w}_0, \quad (2.9)$$

$$\eta \frac{\partial \tilde{\mathbf{w}}_0^-(0)}{\partial r} + \tilde{\mathbf{w}}_1^-(0) = \lim_{\eta \rightarrow -\infty} \mathbf{w}_1 \quad (2.10)$$

and

$$\frac{\eta^2}{2} \frac{\partial^2 \tilde{\mathbf{w}}_0^-(0)}{\partial r^2} + \eta \frac{\partial \tilde{\mathbf{w}}_1^-(0)}{\partial r} + \tilde{\mathbf{w}}_2^-(0) = \lim_{\eta \rightarrow -\infty} \mathbf{w}_2. \quad (2.11)$$

The matched asymptotic analysis now requires that the macroscopic melt velocity should vanish at the each order of ε , i.e. $\tilde{\mathbf{w}}_k^-(0)$ for $k \in (0, 2)$. From equations (2.9)–(2.11), we conclude that the polynomial expansion of the inner melt velocity \mathbf{w} in a series of η , while approaching the solid side of the interface, should not have linear or quadratic terms. Another way to put it is

$$\tilde{\mathbf{w}}_0^-(0) = \frac{\partial \tilde{\mathbf{w}}_0^-(0)}{\partial r} = \frac{\partial \tilde{\mathbf{w}}_1^-(0)}{\partial r} = \frac{\partial^2 \tilde{\mathbf{w}}_0^-(0)}{\partial r^2} = 0. \quad (2.12)$$

In the following, we test the two couplings against the matching conditions (equations (2.9)–(2.11)) via equation (2.9).

We denote the normal and tangential components of the melt velocity by w^s and w^r . Melt fluid dynamical equations at the steady state, in the reference frame of advancing interface and curvilinear orthogonal coordinate system, are as follows [20,21]:

$$\begin{aligned} \rho \left(\frac{w^r}{\varepsilon} \partial_\eta + \frac{w^s}{1 + \varepsilon \eta \kappa} \partial_s \right) w^r - \rho \frac{w^{s2} \kappa}{1 + \eta \varepsilon \kappa} &= -\frac{1}{\varepsilon} \partial_\eta p + \mu_1 \left(\frac{1}{\varepsilon^2} \partial_\eta \eta + \frac{1}{\varepsilon} \kappa \partial_\eta + \partial_{ss} \right) w^r \\ &+ \rho(1 - \gamma u) g^r - h^* \mu_1 \frac{H(\varphi)}{L_d^2 \varepsilon^2} w^r, \end{aligned} \quad (2.13)$$

$$\begin{aligned} \rho \left(\frac{w^r}{\varepsilon} \partial_\eta + \frac{w^s}{1 + \varepsilon \eta \kappa} \partial_s \right) w^s - \rho \frac{w^s w^r \kappa}{1 + \eta \varepsilon \kappa} &= -\frac{1}{1 + \varepsilon \eta \kappa} \partial_s p + \mu_1 \left(\frac{1}{\varepsilon^2} \partial_\eta \eta + \frac{1}{\varepsilon} \kappa \partial_\eta + \partial_{ss} \right) w^s \\ &+ \rho(1 - \gamma u) g^s - h^* \mu_1 \frac{H(\varphi)}{L_d^2 \varepsilon^2} w^s \end{aligned} \quad (2.14)$$

and

$$0 = \frac{1}{\varepsilon} \partial_\eta w^r + \kappa_0 w^r + \frac{1}{1 + \varepsilon \eta \kappa} \partial_s w^s. \quad (2.15)$$

Substituting the expansion of inner variables (φ, u, \mathbf{w} and p), we multiply both sides of equations (2.13), (2.14) and (2.15) by ε^2 and ε , respectively, to compare the terms in the same

order of ε up to the second order. In the zeroth order of ε , equations (2.13), (2.14) and (2.15) yield, respectively,

$$\mu_1 \partial_{\eta\eta} w_0^r - h^* \mu_1 \frac{H(\varphi_0)}{L_d^2} w_0^r = 0, \quad (2.16)$$

$$\mu_1 \partial_{\eta\eta} w_0^s - h^* \mu_1 \frac{H(\varphi_0)}{L_d^2} w_0^s = 0 \quad (2.17)$$

and
$$\partial_\eta w_0^r = 0. \quad (2.18)$$

Together with the no-slip boundary condition at the solid side of the interface, $\lim_{\eta \rightarrow -\infty} \mathbf{w}_0 = 0$, the solution of equations (2.16)–(2.18), valid inside the entire interface, is found as

$$w_0^r = w_0^s = 0. \quad (2.19)$$

From equation (2.9), we see that the macroscopic no-slip boundary condition $\tilde{\mathbf{w}}_0^-(0) = 0$ is satisfied. Next, we collect the terms that are in the first order in ε of equations (2.13)–(2.15). This procedure gives

$$\rho w_0^r \partial_\eta w_0^r = -\partial_\eta p_0 + \mu_1 \partial_{\eta\eta} w_1^r + \kappa \mu_1 \partial_\eta w_0^r - \frac{h^* \mu_1}{L_d^2} [H(\varphi_0) w_1^r + \varphi_1 H'(\varphi_0) w_0^r], \quad (2.20)$$

$$\rho w_0^r \partial_\eta w_0^r = \mu_1 \partial_{\eta\eta} w_1^s + \kappa \mu_1 \partial_\eta w_0^s - \frac{h^* \mu_1}{L_d^2} [H(\varphi_0) w_1^s + \varphi_1 H'(\varphi_0) w_0^s] \quad (2.21)$$

and
$$\partial_\eta w_1^r + \kappa_0 w_0^r + \partial_s w_0^s = 0. \quad (2.22)$$

From the continuity equation at the first order in ε , equation (2.22), and using equation (2.19), we find that $\partial_\eta w_1^r = 0$. Application of no-slip boundary condition $\lim_{\eta \rightarrow -\infty} w_1^r = 0$ reveals that w_1^r identically vanishes inside the interface. Using this information in equation (2.20), we find $\partial_\eta p_0 = 0$, or equivalently $p_0 = \bar{p}$ for an integration constant \bar{p} .

$$w_1^r = w_1^s = 0. \quad (2.23)$$

Thus, the linear coefficient of the inner melt velocity in the first order of ε , when expanded in a series of η , is zero. From equation (2.10), we conclude that the no-slip boundary condition is valid in the sharp interface limit, i.e. $\partial \tilde{\mathbf{w}}_0^-(0)/\partial r = 0$. Finally, we collect the terms that are in the second order in ε of equations (2.13)–(2.15). The second order of ε corresponds to the thin interface limit, which is the main focus of this study. At this second order

$$\begin{aligned} \rho(w_0^r \partial_\eta w_1^r + w_1^r \partial_\eta w_0^r) - \rho \kappa (w_0^s)^2 &= -\partial_\eta p_1 + \mu_1 \partial_{\eta\eta} w_2^r + \mu_1 \partial_{ss} w_0^r + \kappa \mu_1 \partial_\eta w_1^r + \rho(1 - \gamma u_0) g^r \\ &- \frac{h^* \mu_1}{L_d^2} \left[H(\varphi_0) w_2^r + \varphi_1 H'(\varphi_0) w_1^r + \left(\varphi_2 + \frac{1}{2} \varphi_1^2 H''(\varphi_0) \right) w_0^r \right], \end{aligned} \quad (2.24)$$

$$\begin{aligned} \rho(w_0^r \partial_\eta w_1^s + w_1^r \partial_\eta w_0^s) - \rho \kappa w_0^s w_0^r &= -\partial_s p_0 + \mu_1 \partial_{\eta\eta} w_2^s + \mu_1 \partial_{ss} w_0^s + \kappa \mu_1 \partial_\eta w_1^s + \rho(1 - \gamma u_0) g^s \\ &- \frac{h^* \mu_1}{L_d^2} \left[H(\varphi_0) w_2^s + \varphi_1 H'(\varphi_0) w_1^s + \left(\varphi_2 + \frac{1}{2} \varphi_1^2 H''(\varphi_0) \right) w_0^s \right], \end{aligned} \quad (2.25)$$

and
$$\partial_\eta w_2^r + \kappa_0 w_1^r - \eta \kappa_0 \partial_s w_1^s = 0. \quad (2.26)$$

From equations (2.19) and (2.23) in equation (2.26), and the no-slip boundary condition, we conclude $w_2^r = 0$. Using this information in equation (2.24), in addition to equations (2.19) and (2.23), we find $-\partial_\eta p_1 = \rho(1 - \gamma u_0) g^r$ or $p_1 = -\rho(1 - \gamma u_0) g^r \eta + \tilde{p}_1$ for an integration constant \tilde{p}_1 . Similarly, equation (2.25) yields

$$0 = -\partial_s p_0 + \rho(1 - \gamma u_0) g^s + \mu_1 \partial_{\eta\eta} w_2^s - \frac{h^* \mu_1}{L_d^2} H(\varphi_0) w_2^s. \quad (2.27)$$

Equation (2.27) reveals that the evolution equations for melt velocity field (up to second order in ε) do not depend upon curvature or deviations of the phase field from its planar equilibrium

shape. Consequently, the optimum coupling parameter h^* does not have a strong dependence upon curvature or deviations of the phase field from the equilibrium shape [12].

To apply the matching boundary condition for melt velocity, equation (2.12), we need to know the behaviour of w_2^s near the solid side of the boundary. Noting that the polynomial $H(\varphi_0)$ in the drag force vanishes at the either side of the interface, $\lim_{\eta \rightarrow -\infty} H(\varphi_0) = 0$, and at the zeroth order of pressure field p_0 is decoupled from the other variables, we have

$$\lim_{\eta \rightarrow -\infty} \mu_1 \partial_{\eta\eta} w_2^s = -\rho(1 - \gamma u_0) g^s. \quad (2.28)$$

Integrating equation (2.28) with respect to η twice and comparing the coefficient of η^2 to $(1/2)\partial^2 \tilde{w}_2^s / \partial r^2$ to apply the matching condition, equation (2.11) gives, $\partial^2 \tilde{w}_2^s / \partial r^2 = -(\rho(1 - \gamma u_0) g^s / \mu_1)$. Thus, in the presence of gravity, the matching condition on the solid side of the interface is not satisfied in the second order of ε expansion. Within the framework of matched asymptotics, this would imply $\tilde{w}_2^-(0) \neq 0$ indicating an apparent slip on the macroscopic level. Numerical simulations on the other hand, enforce zero melt velocity at the solid boundary and prevent the apparent slip at the interface. Furthermore, the optimum coupling parameter h^* ensures a correct description of the melt velocity in the bulk liquid region. Thus, when only the melt velocity in the bulk liquid region is of concern, the drag force should still provide accurate description of melt velocity in the thin interface limit.

In the following, we show that the problem of satisfying the matching boundary condition on the solid side of the interface can be resolved with the variable viscosity model. The fluid dynamical equations for the variable viscosity model in the curvilinear orthogonal coordinates read as follows:

$$\rho \left(\frac{w^r}{\varepsilon} \partial_\eta + \frac{w^s}{1 + \varepsilon \eta \kappa} \partial_s \right) w^r - \rho \frac{w^s \kappa}{1 + \varepsilon \eta \kappa} = -\frac{1}{\varepsilon} \partial_\eta p + \left(\frac{1}{\varepsilon^2} \partial_\eta (\mu(\varphi) \partial_\eta) + \mu(\varphi) \kappa_0 \frac{1}{\varepsilon} \partial_\eta \right) w^r + \partial_s (\mu(\varphi) \partial_s) w^r + \rho(1 - \gamma u) g^r, \quad (2.29)$$

$$\rho \left(\frac{w^r}{\varepsilon} \partial_\eta + \frac{w^s}{1 + \varepsilon \eta \kappa} \partial_s \right) w^s - \rho \frac{w^s w^r \kappa}{1 + \varepsilon \eta \kappa} = -\partial_s p + \left(\frac{1}{\varepsilon^2} \partial_\eta (\mu(\varphi) \partial_\eta) + \mu(\varphi) \kappa_0 \frac{1}{\varepsilon} \partial_\eta \right) w^s + \partial_s (\mu(\varphi) \partial_s) w^s + \rho(1 - \gamma u) g^s \quad (2.30)$$

$$\text{and} \quad 0 = \frac{1}{\varepsilon} \partial_\eta w^r + \kappa_0 w^r + \frac{1}{1 + \varepsilon \eta \kappa} \partial_s w^s. \quad (2.31)$$

Following a procedure similar to the drag force model, the melt velocity component in the direction normal to the interface can be shown to be identically zero inside the interface. For the variable viscosity model, we consider only the melt velocity component in the tangential direction w^s . For this purpose, it suffices to consider the fluid momentum balance in the tangential direction as described in equation (2.30). Next, we investigate w^s up to the second order in ε to ensure that the matching condition for the no-slip boundary condition is indeed satisfied.

At the zeroth order in ε , equation (2.30) gives $\partial_\eta (\mu(\varphi) \partial_\eta) w_0^s = 0$. Assuming that the melt velocity is decoupled from the phase field variable at the zeroth order, one has $w_0^s = 0$. At the next order in ε , equation (2.30) gives $\partial_\eta (\mu(\varphi) \partial_\eta) w_1^s = 0$. Using expression for variable viscosity, equation (1.9), one finds within integration constants k

$$w_1^s(\eta) = \bar{w}^1(0) + \frac{k}{2\mu_1} \int_0^\eta (1 - \varphi_0) dx, \quad (2.32)$$

where $\bar{w}^1(0)$ is the value of w_1^s at the centre of the interface ($\eta = 0$). The indefinite integral on the right-hand side of equation (2.32) is bounded as $\eta \rightarrow -\infty$. Therefore, the expansion of w_1^s in the Taylor series of η , while approaching the solid side of the interface, does not have a term that is linear in η . In other words, using the matching condition equation (2.10), the no-slip boundary condition is satisfied in the sharp interface limit.

Collecting the terms that are in the second order of ε , equation (2.30) gives

$$0 = \frac{\partial}{\partial \eta} \left(\mu(\varphi_0) \frac{\partial w_2^s}{\partial \eta} \right) + \frac{\partial}{\partial \eta} \left(\mu'(\varphi_0) \varphi_1 \frac{\partial w_1^s}{\partial \eta} \right) + \mu(\varphi_0) \kappa_0 \frac{\partial}{\partial \eta} w_1^s - \partial_s p_0 + \rho(1 - \gamma u_0) g^s. \quad (2.33)$$

The variation of the zeroth order pressure p_0 with respect to the tangential coordinate s is neglected. Using the definition for $\mu(\varphi)$ equations (1.9), (2.32) and asymptotic decay of the first-order phase-field correction φ_1 in the limit $\eta \rightarrow -\infty$ (see equation (A 34)), the second term on the right-hand side of equation (2.33) is an infinitesimal.

$$\begin{aligned} \lim_{\eta \rightarrow -\infty} \left[\frac{\partial}{\partial \eta} \left(\mu'(\varphi_0) \varphi_1 \frac{\partial}{\partial \eta} \right) \right] w_1^s &= \lim_{\eta \rightarrow -\infty} \frac{\partial}{\partial \eta} \left[\left(\mu'(\varphi_0) \varphi_1 \frac{\partial w_1^s}{\partial \eta} \right) \right] \\ &= Ak \lim_{\eta \rightarrow -\infty} \frac{\partial}{\partial \eta} \left[\frac{-2\mu_1}{(1 - \varphi_0)^2} \exp\left(\frac{\sqrt{2}\eta}{L_d}\right) \frac{1 - \varphi_0}{2\mu_1} \right] \\ &= -Ak \lim_{\eta \rightarrow -\infty} \frac{\partial}{\partial \eta} \left[\frac{1}{(1 - \varphi_0)} \exp\left(\frac{\sqrt{2}\eta}{L_d}\right) \right] \\ &= -A \frac{k}{2} \lim_{\eta \rightarrow -\infty} \frac{\partial}{\partial \eta} \left[1 + \exp\left(\frac{\sqrt{2}\eta}{L_d}\right) \right] \approx 0. \end{aligned} \quad (2.34)$$

Now, we insert equation (2.32) in equation (2.33) and integrate with respect to η to obtain

$$C_1 = \left[\mu(\varphi_0) \frac{\partial}{\partial \eta} \right] w_2^s + M\eta, \quad (2.35)$$

where C_1 is an integration constant and $M = \rho_0 g^s (1 - \gamma u_0) + k\kappa_0$ is used for brevity. The linear and quadratic coefficients for expansion of w_2^s in the Taylor series of η can be found from equation (2.35) as

$$\lim_{\eta \rightarrow -\infty} \frac{\partial w_2^s}{\partial \eta} = \lim_{\eta \rightarrow -\infty} [-\eta M + C_1] \left[\frac{1 - \varphi_0(\eta)}{2\mu_1} \right] = 0 \quad (2.36)$$

and

$$\lim_{\eta \rightarrow -\infty} \frac{\partial^2 w_2^s}{\partial \eta^2} = - \lim_{\eta \rightarrow -\infty} \left(M \left[\frac{1 - \varphi_0(\eta)}{2\mu_1} \right] + (M\eta + C_1) \left[\frac{1}{2\mu_1} \right] \frac{\partial \varphi_0}{\partial \eta} \right) = 0. \quad (2.37)$$

Noting that $1 - \varphi_0(\eta)$ vanishes exponentially, we conclude that $\lim_{\eta \rightarrow -\infty} \eta(1 - \varphi_0) = 0$ and $\lim_{\eta \rightarrow -\infty} \eta(\partial \varphi_0 / \partial \eta) = 0$. Equations (2.36) and (2.37) imply that w_2^s approaches a constant value asymptotically as $\eta \rightarrow -\infty$, i.e. w_2^s does not have any linear or quadratic terms in η as $\eta \rightarrow -\infty$.

Comparing equations (2.36) and (2.37) with equation (2.11), we obtain

$$\frac{\partial \tilde{w}_0^s(0)}{\partial r} = 0 \quad (2.38)$$

and

$$\frac{\partial^2 \tilde{w}_0^s(0)}{\partial r^2} = 0. \quad (2.39)$$

Thus, we see that variable viscosity model can satisfy matching condition for inner and outer velocity fields, even in the presence of body forces like gravity.

The solid structure, undergoing phase transformation, experiences a force from the melt in addition to external forces like gravity. This force exerted by the melt is evaluated as the surface integral of the projection of the total stress tensor in a direction normal to the interface. The details in which the melt velocity approaches solid side of the interface, via the stress tensor, might become important in the evaluation of such a force. When the growing solid structure also moves in response to the forces exerted by the melt, the two couplings considered here should be applied carefully.

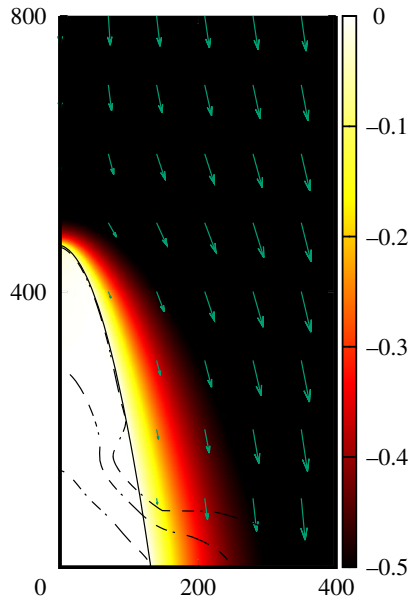


Figure 3. Transient dendrite interface is shown with dashed lines and steady state of the dendrite interface is shown with a solid black line. Colour scheme shows the temperature distribution while arrows show the melt velocity vectors in the steady state. (Online version in colour.)

3. Numerical simulations

To show the equivalence of the two coupling schemes analysed above, numerical investigation of a two-dimensional dendrite growing in the undercooled melt with external melt flow in the opposite direction is carried out. In all of the simulations, we have set the kinetic coefficient $\beta = 0$ by using the thin interface limit relation, equation (A 53). Similar studies have been performed previously with the drag force model [11,14,16].

Initially, a seed is placed in one of the corners of the simulation domain and temperature is set equal to $u_\infty = -\Delta$ everywhere. Type of boundary condition used for temperature and phase field variables is reflective on the sides touching the dendrite and fixed ($\varphi = -1$, $u = u_\infty$) on the sides far from the dendrite. To mimic the situation of the undercooling at infinity, the tip of dendrite is maintained at a constant distance ($2/3$ of the length) from the boundary of the simulation domain.

Anisotropic phase field equation (with anisotropy strength ϵ_4) reads

$$\tau \frac{\partial \varphi}{\partial t} = \nabla \cdot (W^2 \nabla \varphi) + \nabla \cdot \left(|\nabla \varphi|^2 W \frac{\partial W}{\partial \nabla \varphi} \right) + \varphi - \varphi^3 - A_1 \frac{W}{\delta} u (1 - \varphi^2)^2, \quad (3.1)$$

where $\tau = \tau_0 a(\mathbf{n})^2$, $W = W_0 a(\mathbf{n})$, $a(\mathbf{n}) = 1 + \epsilon_4 \cos(4\theta)$ and θ is the angle between normal to the interface and some fixed direction. Lattice Boltzmann (LB) method [22] is used to solve fluid dynamics equations. To avoid the problem due to large viscosity change inside the interface (for the variable viscosity model), two-relaxation-time scheme [23] is chosen for LB equation. For the drag force model, the optimum coupling constant is set to $h^* = 1.31$ [12]. Flow is introduced from top boundary with a fixed velocity and density with the help of Zou–He boundary condition [24].

Figure 3 shows a typical growth of a dendrite along with iso-temperature curves and velocity vector arrows surrounding the dendrite. Temperature iso-lines make it clear that the temperature reaches the undercooling at infinity at a rapid pace, and it is the velocity field that requires a large system size for its spatial gradients to die out.

We now proceed a step further and compare results obtained from numerical simulations to an analytic theory, which makes specific predictions on dimensionless tip velocity of the dendrite,

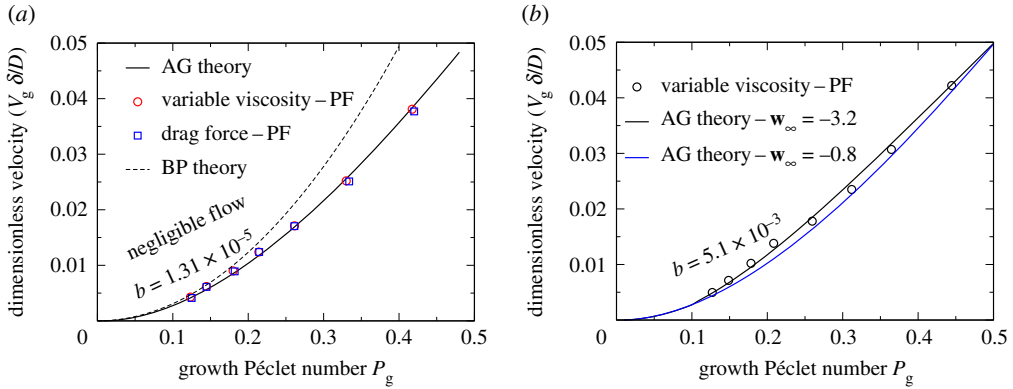


Figure 4. Dimensionless growth velocity of the dendrite tip as a function of growth Péclet number P_g for (a) weak convective transport and (b) strong convective transport. (Online version in colour.)

$\tilde{V}_g = V_g \delta / D$, as a function of the growth Péclet number $P_g = V_g R / 2D$ with R the dendrite tip radius. To obtain different P_g , undercooling at infinity is changed keeping the incoming velocity $|\mathbf{w}_\infty|$ of the melt constant. From the theory of selection of stable mode developed by Alexandrov and Galenko (AG theory) [25,26], the dendrite tip velocity \tilde{V}_g can be predicted as a function of P_g by

$$\tilde{V}_g = \frac{V_g \delta}{D} = \frac{2\sigma_0 \epsilon_4^{7/4}}{1 + b \left(\alpha_{\text{Re}} / \epsilon_4^{3/4} \right)^{11/14}} \cdot \frac{P_g^2}{\left[1 + a_1 \sqrt{\epsilon_4} P_g (1 + \chi D \beta / \delta) \right]^2}, \quad (3.2)$$

where a_1 , χ and σ_0 are the numerical constants, b is the parameter related to the velocity of forced convection, ϵ_4 is the strength of anisotropy (which is the same as in equation (3.1)) and

$$\alpha_{\text{Re}} = \frac{a(\text{Re}) |\mathbf{w}_\infty| \delta}{4R V_g} \quad \text{and} \quad a(\text{Re}) = \sqrt{\frac{\text{Re} \exp(-\text{Re}/2)}{2\pi \operatorname{erfc}(\sqrt{\text{Re}/2})}},$$

with $\text{Re} = |\mathbf{w}_\infty| R / \nu$ the Reynolds number, $\nu = \mu_1 / \rho$ the kinematic viscosity and the expression for $a(\text{Re})$ corresponds to the present two-dimensional case. For the present case of $\beta = 0$, equation (3.2) is [27]

$$\tilde{V}_g = \frac{V_g \delta}{D} = \frac{2\sigma_0 \epsilon_4^{7/4}}{1 + b \left(\alpha_{\text{Re}} / \epsilon_4^{3/4} \right)^{11/14}} \cdot \frac{P_g^2}{\left[1 + a_1 \sqrt{\epsilon_4} P_g \right]^2}. \quad (3.3)$$

A comparison of the theory given by equation (3.3) with simulation results obtained for the two coupling schemes (namely, variable viscosity model and the drag force model) is shown in figure 4. Because the shape of the dendrite deviates from parabola near the dendrite tip due to anisotropic effects [16,28,29], the dendrite radius R is obtained by a fit in a region roughly one radius away from the tip and from the bottom (for the details of deviations of the dendrite surface from the parabolic law behind the dendrite tip see the work [30]).

The result of comparison of the scaled velocity \tilde{V}_g as a function of P_g is shown in figure 4a for phase-field simulations using both types of liquid–solid coupling and analytical predictions using the AG theory and the Bouissou–Pelcé (BP theory) [2]. The corresponding set of physical and simulation parameters used are listed in table 1. Figure 4a shows that variable viscosity and drag force models both yield nearly the same result for all growth Péclet numbers indicating that these two couplings can be used interchangeably for numerical purpose. Furthermore, the phase-field simulation results are in good agreement with the BP theory for relatively low growth Péclet numbers ($P_g \lesssim 0.2$), while the BP theory over-predicts the scaled tip velocity for increasing growth

Table 1. Typical values for the set of parameters in the model (arbitrary units).

parameter	symbol	value	dimension
diffusion coefficient	D	4	$\text{length}^2\text{time}^{-1}$
interface width	W_0	1	length
relaxation time	τ_0	1	time
strength of anisotropy (stiffness)	ϵ_4	5×10^{-2}	—
temperature at infinity	$\Delta(u_\infty)$	−0.55	—
kinematic viscosity	ν	0.16	$\text{length}^2\text{time}^{-1}$
flow velocity at infinity	w_∞	−0.8 and −3.2	$\text{length}\text{time}^{-1}$

Table 2. Dimensionless parameters of the AG equation (3.3).

parameter	$w_\infty = -0.8$	$w_\infty = -3.2$	dimension
stability constant σ_0	29.89	29.89	—
constant a_1	2.083	2.083	—
convective parameter b	1.31×10^{-5}	5.1×10^{-3}	—

Péclet numbers. The AG theory, on the other hand, shows an excellent agreement with the phase-field simulations for the complete range of growth Péclet numbers accessed in the present study. Note that the parameter b in equation (3.3), which characterizes the strength of the convective transport, is very small ($b = 1.31 \times 10^{-5}$) for the data shown in figure 4*a*. To observe the effect of melt flow in simulations more clearly, the far field external velocity is increased by a factor of 4, keeping other physical parameters the same. With a fourfold increase in the external melt velocity the constant b now increases to 5.1×10^{-3} (table 2). Only variable viscosity model has been used to obtain the phase-field results to save the computational effort. Comparison of the phase field and AG theory under this condition of enhanced melt flow is shown in figure 4*b*. As a reference, the analytical curve for the lower external flow velocity using the AG theory is also shown in the same figure. Figure 4*b* shows that the phase-field simulations are in good agreement with the AG theory also in the presence of strong advection effects. Note that, at higher P_g -values, analytical predictions for these two different external melt velocities converge toward each other, which is consistent with experiments and theoretical investigations [31].

4. Conclusion

Through the present analysis, it is shown that the thin interface limit of the phase field equations for solidification problem remains valid even in the presence of the melt flow. Numerical simulations confirm that the two fluid–structure coupling schemes of drag force and variable viscosity analysed in this work, yield the same quantitative results and are in fairly good agreement with theoretical predictions. Within the framework of the present analysis, this suggests that the details of the coupling at the interface do not alter the macroscopic solidification process when the no-slip boundary condition is satisfied. Further extension of the present work to the case of unequal diffusivity and density of the liquid melt and solid phase in the thin interface limit is an interesting topic for future studies.

Data accessibility. This article has no additional data.

Authors' contributions. All the authors have contributed equally to this work.

Competing interests. We declare we have no competing interest.

Funding. P.K.G. acknowledges the support by the European Space Agency (ESA) under research project MULTIPHAS grant no. (AO-2004) and the German Aerospace Center (DLR) Space Management under

Appendix A

(a) Matched asymptotics of temperature and phase-field

More details of the matched asymptotic analysis, specifically different order contributions in the small parameter ε expansion for temperature and phase field, are given in this section. We expand the phase-field variables in a power series of small parameter ε up to the second order as follows:

$$\varphi = \varphi_0 + \varepsilon\varphi_1 + \varepsilon^2\varphi_2, \quad (\text{A } 1)$$

$$u = u_0 + \varepsilon u_1 + \varepsilon^2 u_2, \quad (\text{A } 2)$$

$$V = V_0 + \varepsilon V_1 + V_2 \varepsilon^2, \quad (\text{A } 3)$$

$$f'(\varphi) = f'(\varphi_0) + \varepsilon\varphi_1 f''(\varphi_0) + \varepsilon^2 \left(\varphi_2 f'''(\varphi_0) + \frac{1}{2} \varphi_1^2 f''''(\varphi_0) \right), \quad (\text{A } 4)$$

$$g'(\varphi) = g'(\varphi_0) + \varepsilon\varphi_1 g''(\varphi_0) + \varepsilon^2 \left(\varphi_2 g'''(\varphi_0) + \frac{1}{2} \varphi_1^2 g''''(\varphi_0) \right) \quad (\text{A } 5)$$

and
$$H(\varphi) = H(\varphi_0) + \varepsilon\varphi_1 H'(\varphi_0) + \varepsilon^2 \left(\varphi_2 H'(\varphi_0) + \frac{1}{2} \varphi_1^2 H''(\varphi_0) \right). \quad (\text{A } 6)$$

The aim of the matched asymptotic analysis is to satisfy macroscopic boundary conditions which can be written as follows:

$$\tilde{u}_k^+(0) = -\beta V_k - \delta\kappa_k \quad (\text{A } 7)$$

and

$$V_k = D \frac{\partial \tilde{u}_k^\pm}{\partial r}, \quad (\text{A } 8)$$

where \tilde{u} stands for the macroscopic (outer) reduced temperature field. We start by writing down the corresponding differential operators in the curvilinear orthogonal coordinate system [21,32]

$$\Delta = \frac{1}{\varepsilon^2} \partial_{\eta\eta} + \frac{1}{\varepsilon} \kappa \partial_\eta + (1 - 2\eta\kappa\varepsilon) \partial_{ss} + (\eta\varepsilon) \partial_s, \quad (\text{A } 9)$$

$$\partial_t = \partial_t - \frac{V}{\varepsilon} \partial_\eta + s_t \partial_s, \quad (\text{A } 10)$$

$$\nabla \cdot \mathbf{a} = \frac{1}{\varepsilon} \partial_\eta (\mathbf{r} \cdot \mathbf{a}) + \partial_s (\mathbf{s} \cdot \mathbf{a}) + \kappa_0 (\mathbf{a} \cdot \mathbf{r}) \quad (\text{A } 11)$$

and

$$\nabla = \frac{1}{\varepsilon} \hat{\mathbf{r}} \frac{\partial}{\partial \eta} + \frac{1}{1 + \varepsilon\eta\kappa} \hat{\mathbf{s}} \frac{\partial}{\partial s}. \quad (\text{A } 12)$$

Furthermore, the curvature of the interface is given by

$$\kappa = \Delta r = \kappa_0 + \varepsilon \left(k_1 - \eta\kappa_0^2 \right). \quad (\text{A } 13)$$

Just as the microscopic ones, macroscopic variables are similarly expanded as

$$\begin{aligned} \tilde{u} &\approx \tilde{u}_0 + \varepsilon \tilde{u}_1 + \varepsilon^2 \tilde{u}_2 \\ &= \tilde{u}_0(0) + \varepsilon \left(\eta \frac{\partial \tilde{u}_0(0)}{\partial r} + \tilde{u}_1(0) \right) \\ &\quad + \varepsilon^2 \left(\frac{\eta^2}{2} \frac{\partial^2 \tilde{u}_0(0)}{\partial r^2} + \eta \frac{\partial \tilde{u}_1(0)}{\partial r} + \tilde{u}_2(0) \right). \end{aligned} \quad (\text{A } 14)$$

Comparing the terms of the same orders of ε in equations (A 14) and (A 2), the matching boundary conditions for the reduced temperature field u are

$$\lim_{\eta \rightarrow \pm\infty} u_0 = \tilde{u}_0^\pm(0), \quad (\text{A } 15)$$

$$\lim_{\eta \rightarrow \pm\infty} u_1 = \eta \frac{\partial \tilde{u}_0^\pm(0)}{\partial r} + \tilde{u}_1^\pm(0) \quad (\text{A } 16)$$

and

$$\lim_{\eta \rightarrow \pm\infty} u_2 = \frac{\eta^2}{2} \frac{\partial^2 \tilde{u}_0^\pm(0)}{\partial r^2} + \eta \frac{\partial \tilde{u}_1^\pm(0)}{\partial r} + \tilde{u}_2^\pm(0). \quad (\text{A } 17)$$

In the reference frame of the interface moving with a velocity V at steady state, the reduced temperature and phase-field equations in the curvilinear orthogonal coordinates are

$$\begin{aligned} \left(\frac{\beta}{\delta} + \frac{\omega}{D} \frac{W}{\delta}\right) \varepsilon^2 \left(-\frac{V}{\varepsilon} \partial_\eta \varphi\right) &= \varepsilon^2 \left(\frac{1}{\varepsilon^2} \partial_{\eta\eta} + \frac{\kappa_0}{\varepsilon} \partial_\eta + \kappa_1 \partial_\eta - \eta \kappa_0^2 \partial_\eta\right) \varphi - \frac{1}{L_d^2} [f'(\varphi_0)] \\ &- \frac{1}{L_d^2} \left[\varepsilon \varphi_1 f''(\varphi_0) + \varepsilon^2 \left(\varphi_2 f''(\varphi_0) + \frac{1}{2} \varphi_1^2 f'''(\varphi_0)\right)\right] - \frac{1}{\delta L_d} A_1 \varepsilon u [g'(\varphi_0) + \varepsilon \varphi_1 g''(\varphi_0)] \\ &+ \frac{1}{\delta L_d} A_1 \varepsilon u \left[\varepsilon^2 \left(\varphi_2 g''(\varphi_0) + \frac{1}{2} \varphi_1^2 g'''(\varphi_0)\right)\right] \end{aligned} \quad (\text{A } 18)$$

and

$$-V \varepsilon \partial_\eta u + \varepsilon \partial_\eta (u w^r) + \varepsilon^2 \partial_s (u w^s) + \kappa_0 \varepsilon^2 (u w^r) = D \partial_{\eta\eta} u + D \varepsilon \kappa_0 \partial_\eta u - D \varepsilon^2 \kappa_0^2 \eta \partial_\eta u - \frac{V \varepsilon}{2} \partial_\eta \varphi. \quad (\text{A } 19)$$

(i) The zeroth order in ε

Comparing terms in the zeroth order of ε in the steady-state equations (A 19) and (A 18), zeroth-order contributions of the temperature and phase field can be obtained.

φ at the zeroth order in ε

$$\partial_{\eta\eta} \varphi_0 = \frac{1}{L_d^2} f'(\varphi_0). \quad (\text{A } 20)$$

The solution of equation (A 20) can be determined from the boundary conditions $\lim_{\eta \rightarrow +\infty} \varphi = -1$ and $\lim_{\eta \rightarrow -\infty} \varphi = 1$. With these boundary conditions, φ_0 turns out to be $\varphi_0 = -\tanh(\eta/\sqrt{2}L_d)$.

u at the zeroth order in ε

At the zeroth order of ε , equation (A 19) gives,

$$D \partial_{\eta\eta} u_0 = 0. \quad (\text{A } 21)$$

Furthermore, at the solid side of the interface, gradient of the reduced temperature vanishes. With this information, the solution of equation (A 21) can be written as

$$u_0 = \bar{u}, \quad (\text{A } 22)$$

where \bar{u} is a constant of integration. Thus, to the zeroth order in ε , the reduced temperature field is constant across the interface. Matching to the outer solution, equations (A 15) and (A 22), we have

$$\lim_{\eta \rightarrow \pm\infty} u_0 = \tilde{u}_0^\pm(0). \quad (\text{A } 23)$$

(ii) The first order in ε

The sharp interface limit of the coupled phase-field equations corresponds to matching of inner and outer solutions in the first order of ε . Starting with the phase-field equation, we shall look at the deviations from the equilibrium profiles for the respective variables.

φ at the first order in ε

Collecting the terms in first order of ε in equation (A 18), we have

$$-\frac{\beta}{\delta}V_0\partial_\eta\varphi_0 = \partial_{\eta\eta}\varphi_1 + \kappa_0\partial_\eta\varphi_0 - \frac{1}{L_d^2}f''(\varphi_0)\varphi_1 - \frac{1}{\delta L_d}A_1u_0g'(\varphi_0). \quad (\text{A } 24)$$

With a slight rearrangement of equation (A 24), we obtain

$$-\left(\frac{\beta}{\delta}V_0 + \kappa_0\right)\partial_\eta\varphi_0 + \frac{1}{\delta L_d}A_1u_0g'(\varphi_0) = \left(\partial_{\eta\eta} - \frac{1}{L_d^2}f''(\varphi_0)\right)\varphi_1. \quad (\text{A } 25)$$

The general solution of the second-order differential equation (A 25) is difficult to obtain in a closed form. To proceed further, we note that $\partial_\eta\varphi_0$ is a solution of the homogeneous differential equation

$$\left(\partial_{\eta\eta} - \frac{1}{L_d^2}f''(\varphi_0)\right)\partial_\eta\varphi_0 = 0. \quad (\text{A } 26)$$

Multiplying both sides of equation (A 25) by $\partial_\eta\varphi_0$ and integrating over the interface with respect to η yields

$$-\left(\frac{\beta}{\delta}V_0 + \kappa_0\right)\int_{-\infty}^{\infty}(\partial_\eta\varphi_0)^2 d\eta = -\frac{1}{\delta L_d}A_1u_0\int_{-\infty}^{\infty}g'(\varphi_0)\partial_\eta\varphi_0 d\eta, \quad (\text{A } 27)$$

where we have used the information of equation (A 26). We introduce following definite integrals for convenience:

$$I = \int_{-\infty}^{\infty}(\partial_y\varphi_0)^2 dy, \quad \text{with } y = \frac{\eta}{L_d} \quad (\text{A } 28)$$

and

$$J = \int_{-1}^1 g'(\varphi_0) d\varphi_0 = g(1) - g(-1) = \frac{4}{3}. \quad (\text{A } 29)$$

In addition, choosing $A_1 = I/J$, equation (A 27) can be written as

$$u_0 = -\beta V_0 - \delta\kappa_0. \quad (\text{A } 30)$$

To relate the inner variable u_0 to the outer one \tilde{u}_0 , we use the matching boundary condition for outer variable equation (A 15), to arrive at

$$\tilde{u}_0^\pm(0) = -\delta\kappa_0 - \beta V_0. \quad (\text{A } 31)$$

Equation (A 31) represents the Gibbs–Thomson boundary condition in the sharp interface limit. For later purpose, we need the behaviour of φ_1 near the solid side of the interface to determine the relative smallness of the terms in the velocity field asymptotics. To find out the form of φ_1 , we take the limit $\eta \rightarrow -\infty$ in equation (A 25), and obtain

$$\lim_{\eta \rightarrow -\infty} \left[-\left(\frac{\beta}{\delta}V_0 + \kappa_0\right)\partial_\eta\varphi_0 + \frac{1}{\delta L_d}a_1u_0g'(\varphi_0) \right] = \lim_{\eta \rightarrow -\infty} \left(\partial_{\eta\eta} - \frac{1}{L_d^2}f''(\varphi_0)\right)\varphi_1 \quad (\text{A } 32)$$

with $\varphi_0 = -\tanh(\eta/\sqrt{2}L_d)$ and $g'(\varphi_0) = (1 - \varphi_0^2)^2$, the left-hand side of equation (A 32) is zero. Noting that $f''(\varphi_0) = -(1 - 3\varphi_0^2)$, the left-hand side of the equation is simplified as follows:

$$0 = \lim_{\eta \rightarrow -\infty} \left(\partial_{\eta\eta} - \frac{2}{L_d^2}\right)\varphi_1. \quad (\text{A } 33)$$

The general solution of equation (A 33), that satisfies the boundary condition $\lim_{\eta \rightarrow -\infty} \varphi_1 = 0$, is

$$\lim_{\eta \rightarrow -\infty} \varphi_1 = A \exp\left(\frac{\sqrt{2}\eta}{L_d}\right). \quad (\text{A } 34)$$

u at the first order in ε

At the first order in ε , we seek to obtain macroscopic heat balance condition from the consideration of the reduced temperature field in the sharp interface limit. Equating the terms of the first order in ε in equation (A 19) gives

$$-V_0 \partial_\eta u_0 + \partial_\eta (w_0^r u_0) = D \partial_{\eta\eta} u_1 - \frac{V_0}{2} \partial_\eta \varphi_0. \quad (\text{A } 35)$$

Given that u_0 and w_0^r are constant inside the interface, their spatial derivative with respect to η vanishes. Integration of equation (A 35) with respect to η yields

$$D \partial_\eta u_1 = A + \frac{V_0}{2} \varphi_0, \quad (\text{A } 36)$$

where A is an integration constant. Integrating the above expression once more, we have

$$u_1 = \bar{u} + \frac{A}{D} \eta + \frac{V_0}{2D} \int_0^\eta \varphi_0(x) dx, \quad (\text{A } 37)$$

where \bar{u} is the value of u_1 at the centre of the interface $\eta = 0$. In order to use the matching boundary condition for the reduced temperature field, the behaviour of equation (A 37) near the either ends of the interface needs to be known. Taking the limit $\eta \rightarrow \pm\infty$ of equation (A 37) yields

$$\lim_{\eta \rightarrow \infty} u_1 = \bar{u} + \left(\frac{A}{D} - \frac{V_0}{2D} \right) \eta + \frac{V_0}{2D} \int_0^\eta (1 + \varphi_0(x)) dx \quad (\text{A } 38)$$

and

$$\lim_{\eta \rightarrow -\infty} u_1 = \bar{u} + \left(\frac{A}{D} + \frac{V_0}{2D} \right) \eta + \frac{V_0}{2D} \int_0^\eta (-1 + \varphi_0(x)) dx. \quad (\text{A } 39)$$

Using the boundary condition for matching equation (A 16), and comparing coefficients of η in equations (A 39) and (A 38), we have

$$\frac{\partial \tilde{u}_0^+(0)}{\partial r} = \frac{A}{D} - \frac{V_0}{2D} \quad (\text{A } 40)$$

and

$$\frac{\partial \tilde{u}_0^-(0)}{\partial r} = \frac{A}{D} + \frac{V_0}{2D}. \quad (\text{A } 41)$$

The macroscopic heat balance condition is obtained by subtracting the above two equations. This yields

$$V_0 = D \left(\frac{\partial \tilde{u}_0^-(0)}{\partial r} - \frac{\partial \tilde{u}_0^+(0)}{\partial r} \right). \quad (\text{A } 42)$$

Thus, we conclude that the advection transport term $\nabla \cdot (u\mathbf{w})$ does not violate the heat conservation equation in the sharp interface limit.

(iii) φ at the second order in ε

The second order of ε corresponds to the thin interface limit of the coupled phase-field equations. Collecting the terms in the second order of ε in the expansion equation for the phase-field

equation (A 18), we obtain

$$\begin{aligned} -\frac{\beta}{\delta}(V_0\partial_\eta\varphi_1 + V_1\partial_\eta\varphi_0) - \frac{\omega}{D}V_0\partial_\eta\varphi_0 &= \partial_{\eta\eta}\varphi_2 + \kappa_0\partial_\eta\varphi_1 + \kappa_1\partial_\eta\varphi_0 - \eta\kappa_0^2\partial_\eta\varphi_0 \\ &- \frac{1}{L_d^2}\varphi_2f''(\varphi_0) - \frac{\varphi_1^2}{2L_d^2}f'''(\varphi_0) - \frac{1}{\delta L_d}A_1(u_0\varphi_1g''(\varphi_0) + u_1g'(\varphi_0)). \end{aligned} \quad (\text{A } 43)$$

A slight rearrangement of the terms in equation (A 43) gives

$$\begin{aligned} \left(\partial_{\eta\eta} - \frac{1}{L_d^2}f''(\varphi_0)\right)\varphi_2 &= -\left(\frac{\beta}{\delta}V_0 + \kappa_0\right)\partial_\eta\varphi_1 - \left(\frac{\beta}{\delta}V_1 + \kappa_1\right)\partial_\eta\varphi_0 + \eta\kappa_0^2\partial_\eta\varphi_0 \\ &- \frac{\omega}{D}V_0\partial_\eta\varphi_0 + \frac{\varphi_1^2}{2L_d^2}f'''(\varphi_0) + \frac{1}{\delta L_d}A_1u_0\varphi_1g''(\varphi_0) + \frac{1}{\delta L_d}A_1u_1g'(\varphi_0). \end{aligned} \quad (\text{A } 44)$$

Similar to the case of φ_1 , a closed form solution of equation (A 44) is difficult to obtain. To proceed further, we use the solvability condition [7] to yield

$$\begin{aligned} 0 &= \int_{-\infty}^{\infty} \left[\left(\partial_{\eta\eta} - \frac{1}{L_d^2}f''(\varphi_0) \right) \varphi_2 \right] \partial_\eta\varphi_0 \, d\eta \\ &= -\left(\frac{\beta}{\delta}V_0 + \kappa_0\right) \int_{-\infty}^{\infty} \partial_\eta\varphi_1\partial_\eta\varphi_0 \, d\eta - \left(\frac{\beta}{\delta}V_1 + \kappa_1\right) \int_{-\infty}^{\infty} (\partial_\eta\varphi_0)^2 \, d\eta \\ &\quad + \kappa_0^2 \int_{-\infty}^{\infty} \eta(\partial_\eta\varphi_0)^2 \, d\eta + \int_{-\infty}^{\infty} \frac{\varphi_1^2}{2L_d^2}f'''(\varphi_0)(\partial_\eta\varphi_0) \, d\eta \\ &\quad + \frac{1}{\delta L_d}A_1 \int_{-\infty}^{\infty} u_0\varphi_1g''(\varphi_0)(\partial_\eta\varphi_0) \, d\eta + \frac{1}{\delta L_d}A_1 \int_{-\infty}^{\infty} u_1g'(\varphi_0)(\partial_\eta\varphi_0) \, d\eta. \end{aligned} \quad (\text{A } 45)$$

The equilibrium phase-field profile φ_0 is an odd function of η implying that $\partial_\eta\varphi_0$ is an even function of η . Moreover, we note from equation (A 25), that φ_1 is an even function, which makes $\partial_\eta\varphi_1$ an odd function. Similarly, $f'''(\varphi)$ and $g''(\varphi)$ are odd functions, given that $f(\varphi)$ is a double well-potential function and $g'(\varphi) = (1 - \varphi^2)^2$. Hence, the first and third integrands are odd function of η . This, in turn, implies

$$\left. \begin{aligned} \int_{-\infty}^{\infty} \partial_\eta\varphi_1\partial_\eta\varphi_0 \, d\eta &= \int_{-\infty}^{\infty} \eta(\partial_\eta\varphi_0)^2 \, d\eta = 0 \\ \int_{-\infty}^{\infty} \frac{\varphi_1^2}{2L_d^2}f'''(\varphi_0)(\partial_\eta\varphi_0) \, d\eta &= \int_{-\infty}^{\infty} u_0\varphi_1g''(\varphi_0)\partial_\eta\varphi_0 \, d\eta = 0. \end{aligned} \right\} \quad (\text{A } 46)$$

and

Using equations (A 28), (A 29) and (A 46), (A 45) are simplified to

$$0 = -\left(\frac{\beta}{\delta}V_1 + \kappa_1\right) \frac{I}{L_d} + \frac{1}{\delta L_d}A_1 \int_{-\infty}^{\infty} u_1g'(\varphi_0)\partial_\eta\varphi_0 \, d\eta - \frac{\omega}{D}V_0 \frac{I}{L_d}. \quad (\text{A } 47)$$

Substituting in equation (A 47), the expression for u_1 with the help of equation (A 37), we obtain

$$\begin{aligned} 0 &= -\left(\frac{\beta}{\delta}V_1 + \kappa_1\right) \frac{I}{L_d} + \frac{1}{\delta L_d}A_1\bar{u} \int_{-\infty}^{\infty} g'(\varphi_0)\partial_\eta\varphi_0 \, d\eta \\ &\quad + \frac{1}{\delta^2} \int_{-\infty}^{\infty} \left(\frac{V_0}{2D} \int_0^\eta \varphi_0(x) \, dx \right) g'(\varphi_0)\partial_\eta\varphi_0 \, d\eta. \end{aligned} \quad (\text{A } 48)$$

For further simplification, we note from equations (A 16) to (A 37),

$$\tilde{u}_1^\pm(0) = \bar{u} + \frac{V_0}{2D} \int_0^\infty (1 + \varphi_0(x)) \, dx. \quad (\text{A } 49)$$

Also let

$$F = \int_0^\infty (1 + \varphi_0(x)) \, dx \quad (\text{A } 50)$$

and

$$\begin{aligned} K &= \int_{-\infty}^{\infty} \left(\int_0^{\eta} \varphi_0(x) dx \right) g'(\varphi_0) (\partial_{\eta} \varphi_0) d\eta, \\ &= - \int_{-\infty}^{\infty} g(\varphi_0) \varphi_0 d\eta. \end{aligned} \quad (\text{A } 51)$$

Using the value of \bar{u} from equation (A 49), and identifying definite integrals equations (A 51) and (A 50) in equation (A 48), we arrive at

$$J \frac{A_1}{\delta L_d} u_1^{\pm}(0) = (\beta V_1 + \kappa_1 \delta) \frac{I}{\delta L_d} + \frac{A_1}{\delta^2} \frac{V_0 \delta}{2D} FJ + \frac{V_0}{\delta L_d} \frac{\delta}{2D} K - \omega \frac{V_0 \delta}{D} \frac{I}{\delta L_d}. \quad (\text{A } 52)$$

Using the fact that $A_1 = I/J$, we obtain

$$u_1^{\pm}(0) = -(\beta V_1 + \kappa_1 \delta) + \frac{V_0 \delta}{2D} F + \frac{V_0 \delta}{2D} \frac{K}{I} - \omega \frac{V_0 \delta}{D} = -(\beta V_1 + \kappa_1 \delta) + \frac{V_0 \delta}{2D} \left(F + \frac{K}{I} - 2\omega \right).$$

Equation (A 53) is one of the central results of the present asymptotic expansion analysis, as it gives the relation between the macroscopic undercooling (recall that up to the first order in ε approximation, $u^{\pm}(0) = u_0^{\pm}(0) + \varepsilon u_1^{\pm}(0)$) and the physical parameters of the model. This relation is, however, different from the standard Gibbs–Thomson equation unless the second bracket on the right-hand side of equation (A 53) vanishes. Choosing $\omega = \frac{1}{2}(F + K/I)$, we ensure that Gibbs–Thomson condition also holds at ε^1 order.

In terms of the phase-field parameters, the relation is

$$\beta = \frac{\tau \delta}{W^2} - \frac{\omega W}{D}. \quad (\text{A } 53)$$

Interestingly, equation (A 53) which is the thin interface limit relation in the presence of melt flow turns out to be identical to the one derived for the diffusion limited solidification problem by Karma & Rappel [7].

u at the second order in ε

At the second order in ε , we seek to obtain the heat conservation condition in the thin interface limit. Equating the terms of ε^2 in equation (A 19), one arrives at

$$\begin{aligned} &-V_0 \partial_{\eta} u_1 + V_1 \partial_{\eta} u_0 + \partial_{\eta} (u_1 w_0^r + u_0 w_1^r) + \kappa_0 w_0^r + \partial_s (u_0 w_0^s) \\ &= D \partial_{\eta} \partial_{\eta} u_2 - \frac{V_0}{2} \partial_{\eta} \varphi_1 + D [\kappa_0 \partial_{\eta} u_1 + \kappa_1 \partial_{\eta} u_0] - \frac{V_1}{2} \partial_{\eta} \varphi_0. \end{aligned} \quad (\text{A } 54)$$

We know that the melt velocity in a direction normal to the interface w^r is identically equal to zero at the zeroth and first order of ε , i.e. $w_0^r = w_1^r = 0$ inside the interface. In addition, the tangential melt velocity w_0^s in the first order of ε is also equal to zero due to the no-slip boundary condition. Finally, noting that u_0 is constant inside the interface and integrating equation (A 54) with respect to η , we obtain

$$E - V_0 u_1 = D \partial_{\eta} u_2 + D \kappa_0 u_1 - \frac{V_0}{2} \varphi_1 - \frac{V_1}{2} \varphi_0, \quad (\text{A } 55)$$

where E is a constant of integration. With a slight rearrangement, equation (A 55) can be written as

$$D \partial_{\eta} u_2 = E - (D \kappa_0 + V_0) u_1 + \frac{V_0}{2} \varphi_1 + \frac{V_1}{2} \varphi_0. \quad (\text{A } 56)$$

Integrating equation (A 56) with respect to η , we have

$$D u_2 = D u_2(0) + E \eta - (D \kappa_0 + V_0) \int_0^{\eta} u_1 dx + \frac{V_0}{2} \int_0^{\eta} \varphi_1 dx + \frac{V_1}{2} \int_0^{\eta} \varphi_0 dx, \quad (\text{A } 57)$$

where $u_2(0)$ is the value of u_2 at the centre of the interface ($\eta = 0$). Using the expression for u_1 , equation (A 37), we have

$$Du_2 = Du_2(0) + E\eta + \frac{V_0}{2} \int_0^\eta \varphi_1 dx + \frac{V_1}{2} \int_0^\eta \varphi_0 dx - (D\kappa_0 + V_0) \int_0^\eta \left(\bar{u} + \frac{V_0}{2D} \int_0^x (\varphi_0(z) - 1) dz \right) dx. \quad (\text{A } 58)$$

We write equation (A 58) close to the either end of the interface ($\eta \rightarrow \pm\infty$) separately in order to apply matching conditions

$$\begin{aligned} \lim_{\eta \rightarrow +\infty} Du_2 &= -(D\kappa_0 + V_0) \int_0^\eta \left(\bar{u} - \frac{V_0}{2D}x - \frac{V_0}{2D}x + \frac{V_0}{2D} \int_0^x (\varphi_0 + 1) dy \right) dx \\ &\quad + u_2(0) + E\eta + \frac{V_0}{2} \int_0^\eta \varphi_1 dx + \frac{V_1}{2} \int_0^\eta \varphi_0 dx \\ &= u_2(0) + \frac{V_1}{2} \int_0^\eta (\varphi_0 + 1) dx + \frac{V_0}{2} \int_0^\eta \varphi_1 dx + (D\kappa_0 + V_0) \left(\frac{V_0\eta^2}{2D} \right) \\ &\quad + \left[E - (D\kappa_0 + V_0) \left(\bar{u} + \frac{V_0}{2D} \int_0^{+\infty} (\varphi_0 + 1) dy \right) - \frac{V_1}{2} \right] \eta \end{aligned} \quad (\text{A } 59)$$

and

$$\begin{aligned} \lim_{\eta \rightarrow -\infty} Du_2 &= -(D\kappa_0 + V_0) \int_0^\eta \left(\bar{u} - \frac{V_0}{2D}x + \frac{V_0}{2D}x + \frac{V_0}{2D} \int_0^x (\varphi_0 - 1) dy \right) dx \\ &\quad + u_2(0) + E\eta + \frac{V_0}{2} \int_0^\eta \varphi_1 dx + \frac{V_1}{2} \int_0^\eta \varphi_0 dx \\ &= u_2(0) + \frac{V_1}{2} \int_0^\eta (\varphi_0 - 1) dx + \frac{V_0}{2} \int_0^\eta \varphi_1 dx + \\ &\quad + \left[E - (D\kappa_0 + V_0) \left(\bar{u} + \frac{V_0}{2D} \int_0^{+\infty} (\varphi_0 - 1) dy \right) + \frac{V_1}{2} \right] \eta. \end{aligned} \quad (\text{A } 60)$$

Recalling matching condition for u_2 , equation (A 17), and comparing equations (A 60) and (A 59), one arrives at

$$\lim_{\eta \rightarrow \pm\infty} \tilde{u}_2^\pm(0) = u_2(0) + \frac{V_1}{2} \int_0^\eta (\varphi_0 \pm 1) dx + \frac{V_0}{2} \int_0^\eta \varphi_1 dx. \quad (\text{A } 61)$$

Comparing coefficients of η in equations (A 17), (A 60) and (A 59), we have

$$\frac{\partial \tilde{u}_1^+(0)}{\partial r} = \frac{E}{D} - \left(\kappa_0 + \frac{V_0}{D} \right) \left(\bar{u} + \frac{V_0}{2D} \int_0^\infty (1 + \varphi_0) dx \right) - \frac{V_1}{2D} \quad (\text{A } 62)$$

and

$$\frac{\partial \tilde{u}_1^-(0)}{\partial r} = \frac{E}{D} - \left(\kappa_0 + \frac{V_0}{D} \right) \left(\bar{u} + \frac{V_0}{2D} \int_0^\infty (1 + \varphi_0) dx \right) + \frac{V_1}{2D}. \quad (\text{A } 63)$$

Finally, to arrive at the macroscopic heat balance condition, we subtract equation (A 63) from equation (A 62) to obtain

$$V_1 = D \left(\frac{\partial \tilde{u}_1^-(0)}{\partial r} - \frac{\partial \tilde{u}_1^+(0)}{\partial r} \right). \quad (\text{A } 64)$$

This ensures that, heat conservation condition is also satisfied in the second order of ε . Moreover, comparing coefficients of η^2 in equations (A 17), (A 60) and (A 59), we have

$$\frac{\partial^2 \tilde{u}_0^+}{\partial r^2} = \left(\kappa_0 + \frac{V_0}{D} \right) \frac{V_0\eta^2}{2D} \quad (\text{A } 65)$$

and

$$\frac{\partial^2 \tilde{u}_0^-}{\partial r^2} = 0. \quad (\text{A } 66)$$

Thus, we see that the macroscopic Gibbs–Thomson and energy conservation boundary conditions are valid in the presence of melt flow.

References

1. Ananth R, Gill WN. 1988 Dendritic growth with thermal convection. *J. Cryst. Growth* **91**, 587–598. (doi:10.1016/0022-0248(88)90126-1)
2. Bouissou P, Pelcé P. 1989 Effect of a forced flow on dendritic growth. *Phys. Rev. A* **40**, 6673–6680. (doi:10.1103/PhysRevA.40.6673)
3. Saville D, Beaghton P. 1988 Growth of needle-shaped crystals in the presence of convection. *Phys. Rev. A* **37**, 3423. (doi:10.1103/PhysRevA.37.3423)
4. von Kurnatowski M, Grillenbeck T, Kassner K. 2013 Selection theory of free dendritic growth in a potential flow. *Phys. Rev. E* **87**, 042405. (doi:10.1103/PhysRevE.87.042405)
5. Steinbach I. 2009 Phase-field models in materials science. *Model. Simul. Mater. Sci. Eng.* **17**, 073001. (doi:10.1088/0965-0393/17/7/073001)
6. Caginalp G. 1989 Stefan and Hele-Shaw type models as asymptotic limits of the phase-field equations. *Phys. Rev. A* **39**, 5887–5896. (doi:10.1103/PhysRevA.39.5887)
7. Karma A, Rappel W-J. 1996 Numerical simulation of three-dimensional dendritic growth. *Phys. Rev. Lett.* **77**, 4050. (doi:10.1103/PhysRevLett.77.4050)
8. Echebarria B, Folch R, Karma A, Plapp M. 2004 Quantitative phase-field model of alloy solidification. *Phys. Rev. E* **70**, 061604. (doi:10.1103/PhysRevE.70.061604)
9. Tönhardt R, Gustav A. 1998 Phase-field simulation of dendritic growth in a shear flow. *J. Cryst. Growth* **194**, 406–425. (doi:10.1016/S0022-0248(98)00687-3)
10. Nestler B, Wheeler A, Ratke L, Stöcker C. 2000 Phase-field model for solidification of a monotectic alloy with convection. *Physica D* **141**, 133–154. (doi:10.1016/S0167-2789(00)00035-X)
11. Beckermann C, Diepers H-J, Steinbach I, Karma A, Tong X. 1999 Modeling melt convection in phase-field simulations of solidification. *J. Comput. Phys.* **154**, 468–496. (doi:10.1006/jcph.1999.6323)
12. Subhedar A, Steinbach I, Varnik F. 2015 Modeling the flow in diffuse interface methods of solidification. *Phys. Rev. E* **92**, 023303. (doi:10.1103/PhysRevE.92.023303)
13. Anderson D, McFadden G, Wheeler A. 2001 A phase-field model with convection: sharp-interface asymptotics. *Physica D* **151**, 305–331. (doi:10.1016/S0167-2789(01)00229-9)
14. Tong X, Beckermann C, Karma A, Li Q. 2001 Phase-field simulations of dendritic crystal growth in a forced flow. *Phys. Rev. E* **63**, 061601. (doi:10.1103/PhysRevE.63.061601)
15. Jeong J-H, Goldenfeld N, Dantzig JA. 2001 Phase field model for three-dimensional dendritic growth with fluid flow. *Phys. Rev. E* **64**, 041602. (doi:10.1103/PhysRevE.64.041602)
16. Medvedev D, Fischaleck T, Kassner K. 2006 Influence of external flows on crystal growth: numerical investigation. *Phys. Rev. E* **74**, 031606. (doi:10.1103/PhysRevE.74.031606)
17. Karma A, Rappel W-J. 1998 Quantitative phase-field modeling of dendritic growth in two and three dimensions. *Phys. Rev. E* **57**, 4323. (doi:10.1103/PhysRevE.57.4323)
18. Almgren RF. 1999 Second-order phase field asymptotics for unequal conductivities. *SIAM J. Appl. Math.* **59**, 2086–2107. (doi:10.1137/S0036139997330027)
19. Jamgotchian H, Bergeon N, Benielli D, Voge P, Billia B, Guerin R. 2001 Localized microstructures induced by fluid flow in directional solidification. *Phys. Rev. Lett.* **87**, 166105. (doi:10.1103/PhysRevLett.87.166105)
20. Petrla T, Trif D. 2004 *Basics of fluid mechanics and introduction to computational fluid dynamics*. Berlin, Germany: Springer.
21. Provatas N, Elder K. 2010 *Phase-field methods in materials science and engineering*. Weinheim, Germany: Wiley.
22. Chen S, Doolen G. 1998 Lattice Boltzmann method for fluid flows. *Annu. Rev. Fluid Mech.* **30**, 329–364. (doi:10.1146/annurev.fluid.30.1.329)
23. Ginzburg I, Kuzmin A. 2010 Optimal stability of advection-diffusion lattice Boltzmann models with two relaxation times for positive/negative equilibrium. *J. Stat. Phys.* **139**, 1090–1143. (doi:10.1007/s10955-010-9969-9)
24. Zou Q, He X. 1997 On pressure and velocity boundary conditions for the lattice Boltzmann BGK model. *Phys. Fluids* **9**, 1591–1598. (doi:10.1063/1.869307)

25. Alexandrov DV, Galenko PK. 2015 Thermo-solutal and kinetic regimes of an anisotropic dendrite growing under forced convective flow. *Phys. Chem. Chem. Phys.* **17**, 19149–19161. (doi:10.1039/C5CP03018H)
26. Galenko PK, Reuther K, Kazak O, Alexandrov DV, Rettenmayr M. 2017 Effect of convective transport on dendritic crystal growth from pure and alloy melts. *Appl. Phys. Lett.* **111**, 031602. (doi:10.1063/1.4985340)
27. Alexandrov DV, Galenko PK. 2013 Selection criterion of stable dendritic growth at arbitrary Péclet numbers with convection. *Phys. Rev. E* **87**, 062403. (doi:10.1103/PhysRevE.87.062403)
28. Brener E. 1993 Needle-crystal solution in three-dimensional dendritic growth. *Phys. Rev. Lett.* **71**, 3653–3656. (doi:10.1103/PhysRevLett.71.3653)
29. Brener E. 1999 Pattern formation in three-dimensional dendritic growth. *Physica A* **263**, 338–344. (doi:10.1016/S0378-4371(98)00488-9)
30. Alexandrov DV, Galenko PK. 2020 The shape of dendritic tips. *Phil. Trans. R. Soc. A* **378**, 20190243. (doi:10.1098/rsta.2019.0243)
31. Alexandrov DV, Galenko PK, Toropova LV. 2018 Thermo-solutal and kinetic modes of stable dendritic growth with different symmetries of crystalline anisotropy in the presence of convection. *Phil. Trans. R. Soc. A* **376**, 20170215. (doi:10.1098/rsta.2017.0215)
32. Folch R, Casademunt J, Hernández-Machado A, Ramirez-Piscina L. 1999 Phase-field model for Hele-Shaw flows with arbitrary viscosity contrast. I. Theoretical approach. *Phys. Rev. E* **60**, 1724. (doi:10.1103/PhysRevE.60.1724)